Microsecond Dynamics in Ubiquitin Probed by Solid-State N-15 NMR Spectroscopy R-1 rho Relaxation Experiments under Fast MAS (60-110 kHz)

Author(s):
Lakomek, Nils-Alexander; Penzel, Susanne; Lends, Alons; Cadalbert, Riccardo; Ernst, Matthias; Meier, Beat H.

Publication date:
2017-07-12

Permanent link:
https://doi.org/10.3929/ethz-b-000190282

Originally published in:
Chemistry - A European Journal 23(39), https://doi.org/10.1002/chem.201701738

Microsecond dynamics in ubiquitin probed by solid-state NMR ^{15}N $R_{1\rho}$ relaxation experiments under fast MAS (60-110 kHz)

Nils-Alexander Lakomek, Susanne Penzel, Alons Lends, Riccardo Cadalbert, Matthias Ernst*, Beat H. Meier*

Dr. N. A. Lakomek, S. Penzel, A. Lends, R. Cadalbert, Prof. Dr. M. Ernst, Prof. Dr. B. H. Meier
ETH Zurich, Laboratory of Physical Chemistry
Vladimir-Prelog Weg 2
CH-8093 Zurich
E-mail: maer@ethz.ch; beme@ethz.ch

Abstract: ^{15}N $R_{1\rho}$ relaxation experiments in solid-state NMR are sensitive to timescales and amplitudes of internal protein motions in the hundreds of ns to µs time window, difficult to probe by solution-state NMR. Using ^{15}N $R_{1\rho}$ relaxation experiments we describe a simplified approach to detect low µs protein dynamics and determine residue-specific correlation times from the ratio of ^{15}N $R_{1\rho}$ rate constants at different MAS frequencies. We find that microcrystalline ubiquitin exhibits small-amplitude dynamics on a timescale of about 1 µs across the entire protein, and larger amplitude motions, also on the 1 µs timescale, for several sites, including the β_1-β_2 turn and the N-terminus of the α-helix. According to our analysis, the µs protein backbone dynamics are of lower amplitude than concluded in previous solid-state NMR studies but persist across the entire protein with a rather uniform timescale of 1 µs.

Introduction

Solution-state NMR relaxation measurement have provided important insights into protein dynamics and protein conformational plasticity.[1] While they are sensitive to pico- to nanosecond protein dynamics and relaxation dispersion measurements to micro- to millisecond dynamics,[2] solution-state NMR experiments have a blind spot for dynamics slower than the overall tumbling correlation time of a few ns but faster than about 25 µs,[3] sometimes dubbed supra-τ_c time window.[4] The discussion about the presence/extent of protein dynamics in this supra-τ_c time window, as derived from residual dipolar couplings (RDCs) based measurements, has still not entirely been settled.[5]

During the last two decades, dynamics in proteins have been of considerable interest also in solid-state NMR.[6] Different from solution-state NMR, solid-state NMR relaxation is not restricted by an overall tumbling correlation time.[7] With the introduction of proton detection in biological high-resolution solid-state NMR, also NMR relaxation experiments using the ^{15}N nucleus of the backbone amide group became feasible in solid samples,[8] therefore, allowing similar methodology as is used in solution-state NMR. Proton-detection was achieved first using high levels of deuteration at moderate MAS frequencies,[9] and more recently, utilizing increasingly faster MAS frequencies, also for proteins with lower deuteration levels or even fully protonated samples.[10]

While the absence of an overall tumbling limitation in solid-state NMR allows the study of a wider time range of motions, the incomplete averaging of anisotropic interactions by MAS leads also to coherent time evolution (e.g. under the dipolar coupling) which need to be separated from *true* internal dynamics, therefore complicating the extraction of dynamic information from solid-state NMR data.[7] Longitudinal relaxation rate constants (^{15}N R_1) are relatively straight-forward to measure but the extraction of transverse relaxation-rate constants has turned out to be more difficult, and T_2' (spin echo) experiments are often dominated by coherent effects. However, similar information can be obtained from ^{15}N $R_{1\rho}$ experiments.[11]

Here, we report the MAS-frequency dependence observed for ^{15}N $R_{1\rho}$ rate constants in microcrystalline ubiquitin and interpret the data in terms of the internal dynamics in the hundreds of ns to low µs time range. We show that fast and slow timescales can be treated separately to good approximation, allowing for a simplified approach to detect ns-µs dynamics from the ratio of $R_{1\rho}$ rate constants at different MAS frequencies. Results are validated comparing to a full extended model-free approach for data evaluation.[12] In the MAS-frequency range between 60 and 110 kHz, $R_{1\rho}$ thus provides information about dynamics in the "blind spot" between solution-state NMR relaxation and relaxation-dispersion experiments.

Results and Discussion

^{15}N $R_{1\rho}$ rate constants were measured for uniformly [^2H, ^{13}C, ^{15}N] -labeled microcrystalline ubiquitin (100% of NH back-exchanged, crystallized in 2-Methyl-2,4-pentanediol (MPD)) at a magnetic field strength of 20 T, corresponding to a ^1H Larmor frequency of 850 MHz, and MAS frequencies of 60, 90 and 110 kHz. The spin-lock RF amplitude was set to 13 kHz and the sample temperature to 23±1°C, as described in detail in the Experimental section and Supporting Information.
A strong dependence of ^{15}N $R_{1\rho}$ rate constants on the MAS frequency is observed (Figure 1a), with lower ^{15}N $R_{1\rho}$ rate constants at higher MAS frequencies. For comparison, also the ratio of ^{15}N $R_{1\rho}$ rate constants at 60 and 110 kHz MAS frequency is plotted in Figure 1c. There are three possible explanations for our observations, which were investigated in detail:

1. Coherent contributions (e.g. dipolar interactions) are not sufficiently averaged out and the MAS frequency dependence reflects the residual interactions, with slower decay rates at higher MAS frequencies.

2. A temperature effect: Increased MAS frequencies can lead to an increased heating of the rotor and, therefore, need to be compensated by sufficient cooling. If the temperature between different experiments differs significantly, the change in ^{15}N $R_{1\rho}$ rate constants might be explained by a trivial temperature effect.

3. A true relaxation effect: as ^{15}N $R_{1\rho}$ rate constants contain spectral-density terms at the sum and difference of the MAS frequency ω_r, $2\omega_r$ and the spin-lock frequency, ω_1, (see Eq. 1, below) ^{15}N $R_{1\rho}$ rate constants are sensitive to motions in a time range corresponding to the inverse of these frequencies, which is, at the given MAS frequencies around 100 kHz, the low µs time range.

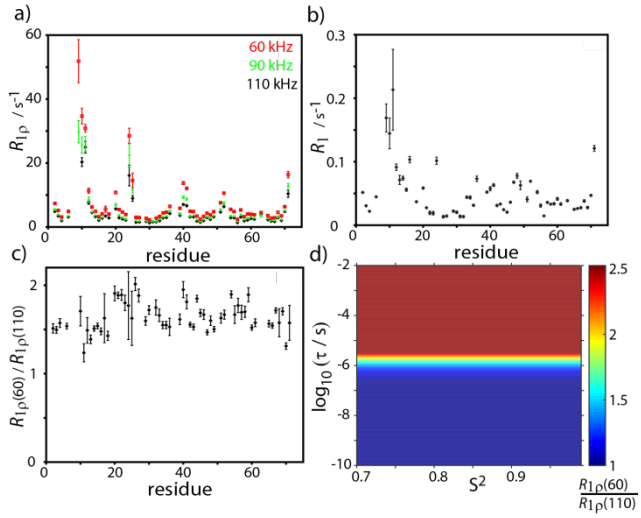

Figure 1. ^{15}N $R_{1\rho}$ and R_1 rate constants measured for [^{2}H, ^{13}C, ^{15}N] -labeled ubiquitin with 100% of NH and exchangeable side-chain protons back-exchanged. Experiments were conducted at 850 MHz and 23±1°C, the spin-lock RF amplitude was 13 kHz. a) ^{15}N $R_{1\rho}$ rate constants measured at 60 kHz (red), 90 kHz (green) and 110 kHz MAS frequency (black). b) ^{15}N R_1 rate constants measured at 110 kHz MAS. c) Experimental ratio of ^{15}N $R_{1\rho}$ rate constants at 60 kHz and 110 kHz. d) Simulated ratio of ^{15}N $R_{1\rho}$ at 60 kHz MAS versus 110 kHz MAS, $R_{1\rho}$(60 kHz)/$R_{1\rho}$(110 kHz) (with a fixed spin-lock RF amplitude of 13 kHz), as a function of order parameter, S^2, and the correlation time, τ_c (logarithmic scale).

1. Coherent contributions to ^{15}N $R_{1\rho}$ rate constants

A possible explanation of decreasing apparent ^{15}N $R_{1\rho}$ rate constants with increasing MAS frequency could be coherent contributions, e.g. dipolar interactions, which may not be sufficiently averaged out even at MAS frequencies greater or equal to 60 kHz. Indeed, coherent spin-spin interactions can, in principle, provide an alternative decay mechanism during the relaxation period and could be mistaken for a relaxation effect. However, as demonstrated by Lewandowski et al., for MAS frequencies of 60 kHz or higher the coherent spin-spin contribution to the measured ^{15}N $R_{1\rho}$ relaxation rate constants should be negligible, even for a fully protonated protein.[11b] In the present study we used [^{2}H, ^{13}C, ^{15}N]-labeled ubiquitin with only amides fully protonated, thus the proton network is strongly diluted and any coherent contributions should be further reduced. We use MAS frequencies of 60 kHz and higher and a spin-lock RF amplitude of 13 kHz far from any rotary-resonance or other recoupling conditions. Therefore, the contribution of coherent time evolution to the measured ^{15}N $R_{1\rho}$ rate constant should be negligible under our experimental conditions.
Nevertheless, we repeated our measurements on [^{2}H, ^{13}C, ^{15}N]-labeled ubiquitin where only 20% of the amides are back exchanged (NH 20%, others contain deuterium instead of the amide proton). Further, MPD, used for crystallization, was also deuterated. This strongly further dilutes the proton network and any coherent interactions will be even more reduced.

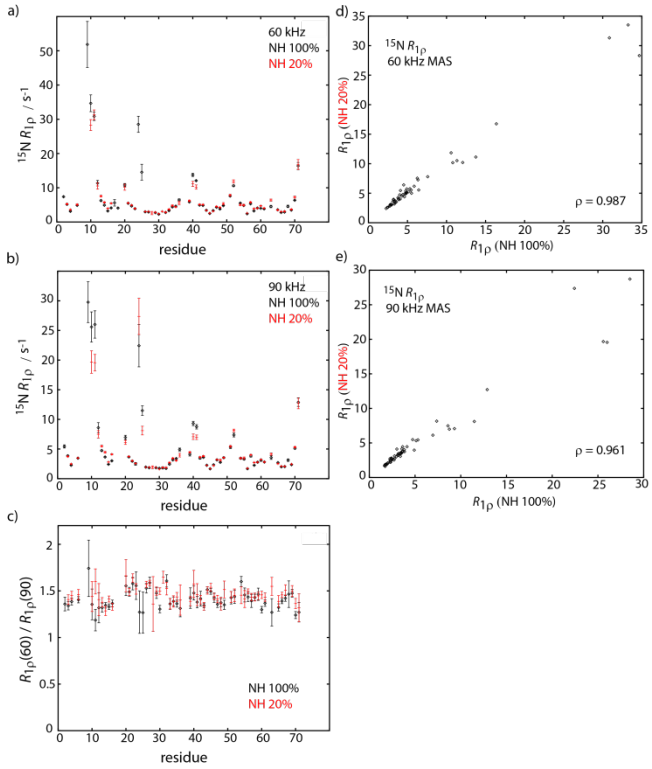

Figure 2. Comparison of ^{15}N $R_{1\rho}$ rate constants measured on [^{2}H, ^{13}C, ^{15}N] -labeled ubiquitin with 100% of NH back-exchanged (black) and NH(20%) protonated (red). Both samples were measured at 850 MHz static field and (a) 60 kHz MAS frequency, (b) 90 kHz MAS and a spin-lock RF amplitude of 13 kHz used in all experiments. c) Ratio of ^{15}N $R_{1\rho}$ rate constants ($R_{1\rho}$(60 kHz)/$R_{1\rho}$(90 kHz)) for the NH(20%) sample and NH(100%) sample. Correlations between ^{15}N $R_{1\rho}$ recorded for NH(100%) and NH(20%) ubiquitin at (d) 60 kHz MAS and (e) 90 kHz MAS. The Pearson correlation coefficient, ρ, for data on NH(100%) versus data on NH(20%) is shown.

Using the 20% back-exchanged sample, we performed measurements at 60 and 90 kHz MAS frequencies using a 13 kHz spin-lock RF amplitude. As shown in Figure 2, both at 60 and 90 kHz MAS ^{15}N $R_{1\rho}$ rate constants for the 20% back-exchanged samples agree well with the data from fully back-protonated samples, which speaks against coherent contributions causing the observed MAS dependence. Also, the residue-specific ratios of ^{15}N $R_{1\rho}$ rate constants at 60 kHz and 90 kHz MAS matches very closely the ratios observed for 100% back-exchanged sample (compare Figure 2c). The C-terminus of ubiquitin, Arg 72 to Gly 76, is invisible in solid-state NMR experiments, attributed to large amplitude internal dynamics,[10e] as observed in solution-state NMR experiments.[13]

2. Temperature effect

^{15}N $R_{1\rho}$ rate constants indeed show temperature dependence as illustrated in Figure S4a and a difference of sample temperature at the different MAS frequencies may lead to systematic errors in the interpretation of the data or even mimic motions that are not present. Therefore, care needs to be taken to compare experiments at the same sample temperature. To internally measure the temperature, the resonance frequency of the supernatant water was used (Figure S5).[14] Furthermore, a temperature-compensation block during experiments (see Supporting Information, Material and Methods and Figure S1) ensured that for each relaxation delay, which was measured in an inter-leaved manner, the same RF power is deposited into the probe, such that the sample temperature will be equilibrated and constant during measurements. Thus, the observed MAS dependence of ^{15}N $R_{1\rho}$ rate constants cannot be explained by a temperature effect either.

3. Dynamics

In contrast to solution-state NMR where the spectral density $J(\omega_1)$ is the dominant contribution for ^{15}N $R_{1\rho}$ (with the spin-lock amplitude ω_1) and frequently the approximation $J(\omega_1) \approx J(0)$ is used, in solid-state NMR sidebands caused by the MAS rotation introduce an additional frequency dependence, and $J(\omega_1)$ is replaced by spectral-density terms which depend on the sum and difference of the spin-lock amplitude, ω_1, and multiples of the MAS frequency, ω_r.[15] On- and off-resonance ^{15}N $R_{1\rho}$ rate constants in solid-state NMR can be described as follows:[15]

$$R_{1\rho} = (R_1^{\mathrm{NH}} + R_1^{\mathrm{CSA}}) + \sin^2\theta \left(R_{1\Delta}^{\mathrm{NH}} + R_{1\Delta}^{\mathrm{CSA}} - \frac{1}{2}(R_1^{\mathrm{NH}} + R_1^{\mathrm{CSA}}) \right) \quad (1a)$$

with

$$R_1^{\mathrm{NH}} = \left(\frac{\delta_{\mathrm{D}}}{4}\right)^2 \left(J(\omega_{\mathrm{N}} - \omega_{\mathrm{H}}) + 3J(\omega_{\mathrm{N}}) + 6J(\omega_{\mathrm{N}} + \omega_{\mathrm{H}}) \right) \quad (1b),$$

$$R_1^{\mathrm{CSA}} = \frac{3}{4}(\delta\omega_{\mathrm{N}})^2 J(\omega_{\mathrm{N}}) \quad (1c),$$

$$R_{1\Delta}^{\mathrm{NH}} = \left(\frac{\delta_\mathrm{D}}{4}\right)^2 \left(3\,J(\omega_\mathrm{H}) + \frac{1}{3}\,J(\omega_1 - 2\omega_\mathrm{r}) + \frac{2}{3}\,J(\omega_1 - \omega_\mathrm{r}) + \frac{2}{3}\,J(\omega_1 + \omega_\mathrm{r}) + \frac{1}{3}\,J(\omega_1 + 2\omega_\mathrm{r})\right), \quad (1\mathrm{d})$$

$$R_{1\Delta}^{\mathrm{CSA}} = \frac{1}{6}(\delta\omega_\mathrm{N})^2 \left(\frac{1}{2}\,J(\omega_1 - 2\omega_\mathrm{r}) + J(\omega_1 - \omega_\mathrm{r}) + J(\omega_1 + \omega_\mathrm{r}) + \frac{1}{2}\,J(\omega_1 + 2\omega_\mathrm{r})\right) \quad (1\mathrm{e}),$$

where the superscript "NH" refers to the dipolar contribution and "CSA" refers to the CSA contribution to the relaxation-rate constant. The terms $J(\omega)$ are the spectral densities of the motion, with the proton Larmor frequency ω_H and the nitrogen Larmor frequency ω_N, the anisotropy of the dipolar coupling $\delta_\mathrm{D} = -2\,\frac{\mu_0}{4\pi}\frac{\gamma_\mathrm{H}\gamma_\mathrm{N}\hbar}{r_\mathrm{NH}^3}$ and the ^{15}N chemical-shift anisotropy $\delta\omega_\mathrm{N}$; here, θ is the angle between the effective field $B_{1,\mathrm{eff}}$ and the external static magnetic field.

^{15}N $R_{1\rho}$ contains a ^{15}N R_1 contribution accounting for off-resonance effects and one further Larmor-frequency term, $J(\omega_\mathrm{H})$, which contributes also under on-resonance conditions (compare Eq. 1a and 1d). The high-frequency term $J(\omega_\mathrm{H})$ samples the spectral density at a very similar frequency as the terms $J(\omega_\mathrm{N} - \omega_\mathrm{H})$ and $J(\omega_\mathrm{N} + \omega_\mathrm{H})$ that contribute to ^{15}N R_1 (Eq. 1b). Because ω_N and ω_H have different signs, it holds that $3J(\omega_\mathrm{H}) < J(\omega_\mathrm{N} - \omega_\mathrm{H}) + 6\,J(\omega_\mathrm{N} + \omega_\mathrm{H})$. Therefore, we can estimate an upper boundary on the maximum high-frequency contribution to ^{15}N $R_{1\rho}$ by measuring ^{15}N R_1 rate constants (which are in first-order approximation expected to be MAS-frequency independent according to Eq. 1b). As shown in Figure 1b, the observed ^{15}N R_1 rate constants in microcrystalline ubiquitin are about two orders of magnitude smaller than ^{15}N $R_{1\rho}$ rate constants (compare Figure 1a), which is very different from e.g. ubiquitin studied by solution-state NMR.[13, 16] Therefore, the ^{15}N R_1 contribution as well as the high-frequency term $J(\omega_\mathrm{H})$ in Eq. 1 can be neglected unless $\sin\theta$ deviates significantly from 1 in the case of severe off-resonance effects. At the maximum offset of $\Delta\Omega$ =15 ppm from the ^{15}N carrier frequency corresponding to 1275 Hz on a 20 T magnet and the applied spin-lock RF amplitude of 13 kHz, the deviation of the effective field $B_{1,\mathrm{eff}}$ from the direction of the B_1 field is still small; this is described by an azimuthal angle $\theta = \arctan\frac{\omega 1}{\Delta\Omega}$ close to 90° and $\sin^2\theta \approx 0.99$, close to 1.

Therefore Eq. 1 can be simplified to:

$$R_{1\rho} \approx R_{1\Delta}^{\mathrm{NH}} + R_{1\Delta}^{\mathrm{CSA}} \quad (2)$$

The term $3\,J(\omega_\mathrm{H})$ for $R_{1\Delta}^{\mathrm{NH}}$ is the only high-frequency term in $R_{1\rho}$ and contributes only very little as discussed above. Thus, neglecting all contributions that sample the spectral density at multiples of the Larmor frequencies, we arrive at:

$$R_{1\rho} \approx \left(\frac{\delta_\mathrm{D}}{4}\right)^2 \left(\frac{1}{3}\,J(\omega_1 - 2\omega_\mathrm{r}) + \frac{2}{3}\,J(\omega_1 - \omega_\mathrm{r}) + \frac{2}{3}\,J(\omega_1 + \omega_\mathrm{r}) + \frac{1}{3}\,J(\omega_1 + 2\omega_\mathrm{r})\right) + \frac{1}{6}(\delta\omega_\mathrm{N})^2 \left(\frac{1}{2}\,J(\omega_1 - 2\omega_\mathrm{r}) + J(\omega_1 - \omega_\mathrm{r}) + J(\omega_1 + \omega_\mathrm{r}) + \frac{1}{2}\,J(\omega_1 + 2\omega_\mathrm{r})\right) \quad (3)$$

Therefore, ^{15}N $R_{1\rho}$ is mainly sensitive to dynamics at the inverse of the sum and difference of spin-lock frequency, ω_1, and MAS frequency, ω_r. We fit the experimental data using a model-free approach, which characterizes the internal dynamics by an order parameter, S^2, (amplitude of motion) and an internal correlation time, τ (timescale of motion).[12] The spectral density $J(\omega) = \frac{2}{5}(1 - S^2)\frac{\tau}{1+(\omega\tau)^2}$, is most sensitive to motions with a time constant similar to the inverse of the frequency ω (plus or minus one order of magnitude) (compare Figure S6 for illustration). Therefore, ^{15}N $R_{1\rho}$ rate constants are sensitive to motions with a time constant similar to the inverse of the MAS frequency (plus or minus two orders of magnitude). Thus, under the conditions of our experiment (60–110 kHz MAS, 13 kHz rf-field amplitude) we are particularly sensitive to dynamics in the hundreds of nanoseconds to low microsecond range which gives the largest contribution to ^{15}N $R_{1\rho}$ (Figure 3a) and the µs time window of protein dynamics becomes accessible. In contrast, earlier studies (e.g. refs. [17]) were more sensitive to a timescale of hundreds of microseconds up to a few milliseconds (Figure 3b) due to the use of lower MAS frequencies.

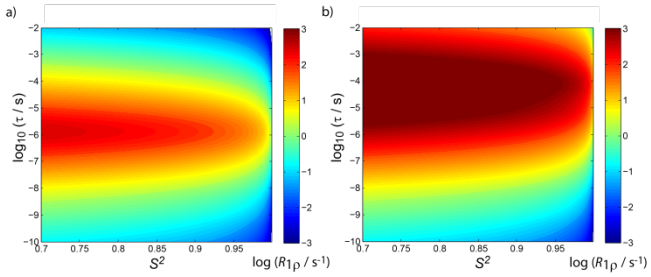

Figure 3. Sensitivity of MAS dependent ^{15}N $R_{1\rho}$ rate constants to protein dynamics. ^{15}N $R_{1\rho}$ rate constants are plotted for (a) 110 kHz MAS and 13 kHz spin-lock RF amplitude (the conditions of our experiment) and (b) 10 kHz MAS and 8 kHz spin-lock RF amplitude.

Simplification of model-free analysis; Timescale information from ratio of ^{15}N $R_{1\rho}$ rate constants

As ^{15}N R_1 relaxation is mainly determined by fast motions and ^{15}N R_1 is experimentally found to be two orders of magnitude smaller than ^{15}N $R_{1\rho}$, and ^{15}N $R_{1\rho}$ values are dominated by motions on slower timescales (hundreds of ns to µs, see above), this allows for a separation of timescales. Therefore, instead of the full extended model-free approach

$$J(\omega) = \frac{2}{5}\left(1 - S_f^2\right)\frac{\tau_f}{1+(\omega\tau_f)^2} + \frac{2}{5}S_f^2(1 - S_s^2)\frac{\tau_s}{1+(\omega\tau_s)^2} \qquad (4),$$

that describes the spectral-density function by two timescales of motion, a fast timescale characterized by an order parameter S_f^2 and a correlation time τ_f and a slow timescale, characterized by S_s^2 and τ_s ,[12] we fit the ^{15}N $R_{1\rho}$ data by a two-parameter model, describing only the slow timescale (S_s^2, τ_s) defined by the spectral-density function

$$J(\omega) = \frac{2}{5}S_f^2(1 - S_s^2)\frac{\tau_s}{1+(\omega\tau_s)^2} \qquad (5).$$

The pre-factor S_f^2 in Eq. 5 can be extracted from an overall order parameter $S_{REDOR}^2 = S_f^2 S_s^2$, see below.

As ^{15}N $R_{1\rho}$ is linear in the spectral densities (see Eq. 1), we can place the order parameter $(1 - S_s^2)$ outside the brackets in this approximation (Eq. 6), such that it cancels out for the ratio of ^{15}N $R_{1\rho}$ rate constants at different MAS frequencies:

$$R_{1\rho} \approx \frac{2}{5}S_f^2(1 - S_s^2)\cdot\left\{\left(\frac{\delta_D}{4}\right)^2\left(\frac{1}{3}\frac{\tau_s}{1+((\omega_1-2\omega_r)\tau_s)^2} + \frac{2}{3}\frac{\tau_s}{1+((\omega_1-2\omega_r)\tau_s)^2} + \cdots\right) + \frac{1}{6}(\delta\omega_N)^2\left(\frac{1}{2}\frac{\tau_s}{1+((\omega_1-2\omega_r)\tau_s)^2} + \cdots\right)\right\} \quad (6)$$

In this approximation, the ratio of ^{15}N $R_{1\rho}$ rate constants measured at different MAS frequencies depends only on the slow timescale correlation time, τ_s. Under our experimental conditions, dynamics slower than about $\tau_s = 10^{-5}$ s will give a ^{15}N $R_{1\rho}$ ratio for MAS at 60 kHz/110 kHz close to 2.5, while dynamics faster than about $\tau_s = 10^{-7}$ s will give a ratio close to 1 (Figure 1d). The experimentally observed ratio of ^{15}N $R_{1\rho}$ (60 kHz/110 kHz), lies in the range between 1.3 to 2 for most residues (Figure 1c), which indicates the presence of µs dynamics with a correlation time around $\tau_s = 1 \cdot 10^{-6}$ s (see Figure 1c and 1d). By using the ratio of ^{15}N $R_{1\rho}$ rate constants, the fitting problem is reduced to a one-parameter fit, with τ_s as the only free parameter. We simultaneously fit three ratios of ^{15}N $R_{1\rho}$ rate constants (60 kHz/110 kHz, 90 kHz/110 kHz, 60 kHz/90 kHz) using a grid-based approach, as described in detail in the Experimental section. Indeed, as expected from the above arguments, residue-specific correlation times, τ_s, are obtained that fall in the 1-2 µs range (Figure 4a).

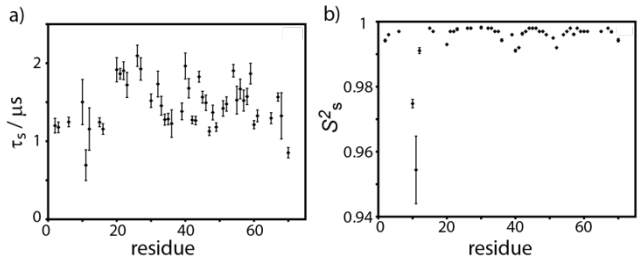

Figure 4. Timescales and amplitudes of motion as extracted from the model-free analysis. a) Residue specific internal correlation times, τ_s, as fitted to the ratio of ^{15}N $R_{1\rho}$ values. b) Order parameters, S_s^2, characterize the amplitude of internal dynamics for each residue.

Next, the ^{15}N $R_{1\rho}$ rate constants, obtained at 60, 90 and 110 kHz MAS frequency, were fitted with an order parameter S_s^2 by Eq. 5, using the correlation times τ_s (as determined by the fit of ratios of ^{15}N $R_{1\rho}$ rate constants, see above) as a fixed input parameter; thus, the order parameter S_s^2 is the only free parameter (Figure 4b)). We calculate the pre-factor S_f^2 in Eq. 5 from an overall order parameter $S_{\mathrm{REDOR}}^2 = S_f^2 S_s^2$ as determined by Haller and Schanda using an improved ^{15}N REDOR measurement.[18] Our results show, however, little dependence on S_f^2. Even when entirely neglecting the fast timescale by setting $S_f^2 = 1$ the obtained S_s^2 are very similar (Figure S7).

We tested the validity of our approximation, separating fast and slow timescale: If the amplitude of µs dynamics (τ_s = 1 µs) is small (S_s^2 = 0.998) then the corresponding ^{15}N $R_{1\rho}$ rate constants will also be small. As a consequence, also dynamics on the ns timescale can contribute to the ^{15}N $R_{1\rho}$ rate constants and the fast timescale, characterized by τ_f and S_f^2, cannot be neglected. The error introduced by neglecting the fast timescale is plotted in Figure S8a as a function of τ_f and S_f^2. As an example, dynamics on the τ_f = 1 ns timescale with an order parameter S_f^2=0.9 would contribute a relative amount of about 20% to the ^{15}N $R_{1\rho}$ rate constant and would, therefore, introduce an error of 20% when neglected (compare Figure S8a). When the amplitude of the 1 µs motion is larger (S_s^2 = 0.995) the relative error will go down to 10% (Figure S8b), to about 5% for S_s^2 = 0.99 (Figure S8c) and about 1% for S_s^2 = 0.95 (Figure S8d). However, those ns dynamics would also have a significant contribution to the ^{15}N R_1 rate constants (Figure S9). When comparing the simulated ^{15}N R_1 rate constants (Figure S9) with experimentally observed ones (Figure 1b), we find that, in the case of microcrystalline ubiquitin, ^{15}N R_1 rate constants rarely exceed values of 0.15 s^{-1}. Only for the first loop region we find larger values while for most residues rate constants stay well below 0.05 s^{-1}. Therefore, for the residues where we find low-amplitude backbone dynamics on the 1 µs timescale (S_s^2 = 0.998), the low experimental ^{15}N R_1 rate constants exclude the presence of high-amplitude ns dynamics with an order parameter S_f^2 < 0.95 and a timescale in the 1 to 10 ns range (compare Figure S9c). Thus, the small experimentally observed ^{15}N R_1 rate constants argue against the presence of high-amplitude ns dynamics, as those ns dynamics should also be sampled by spectral densities contributing to ^{15}N R_1 rate constants and therefore would lead to higher ^{15}N R_1 rate constants than observed. Note further that if there were large-amplitude dynamics on the ns timescale they would not show the

observed MAS dependence of ^{15}N $R_{1\rho}$ (because that timescale is far away from the MAS timescale and, therefore, contributes only little to the respective spectral densities, for nanosecond dynamics the $J(\omega_H)$ term would have the biggest contribution).

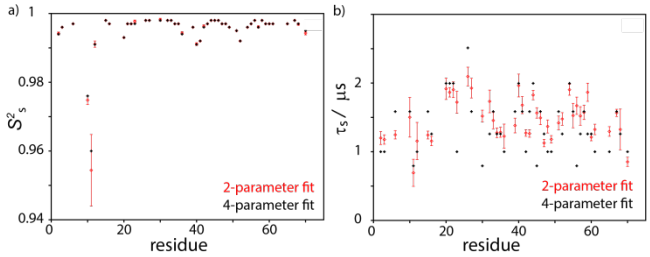

Figure 5. Comparison of slow timescale order parameters, S_s^2 , and correlation times, τ_s, fitted using the two-parameter fit (red) and fitted using the four-parameter fit (black) a) S_s^2 and b) τ_s.

Our data-evaluation procedure was cross-validated by performing a four-parameter fit that besides the ^{15}N $R_{1\rho}$ rate constants included also ^{15}N R_1 rate constants and S^2_{REDOR} order parameter (from the literature[18]) as experimental input data. The four-parameter fit uses simultaneously fast-timescale and slow-timescale order parameters and correlation times as fitting parameters. A comparison between four-parameter fit and two-parameter fit shows that both approaches find very similar solutions for the slow timescale order parameter S_s^2 and correlation time τ_s (Figure 5). Therefore, a separation of timescales and the simplifications applied for the two-parameter fit seem justified, corroborating the finding of 1 µs timescale dynamics in microcrystalline ubiquitin.

Amplitudes of motion and "rocking motions"

For the major part of ubiquitin, the observed microsecond dynamics in the 1-2 µs range are of small amplitude, with a semi-cone opening angle $\theta < 4°$ in the restricted rotational diffusion (*diffusion in a cone*) model or a jump angle in a two-site jump model (both states equally populated) of about $\theta \approx 2°$ (Figure 6). Our results differ significantly from previous studies in that we find a rather uniform timescale in the low µs range and that motions are of small amplitude for most residues but distributed across the entire protein.[17b, 18-19] For a more detailed discussion of the previous literature we refer to the Supporting Information. Our results of low amplitude backbone dynamics in the low µs range are similar to recent findings for HET-s(218-289) fibrils.[20] Results from HET-s(218-289) do differ from those here, in that an $R_{1\rho}$-only analysis resulted in distortion of the S^2 values when nanosecond motion was not included in the model. However such distortion is only expected when significant nanosecond motion is present, and in fact estimation of the correlation time was still fairly accurate, having changed by only a factor 2-3. [20]

It was recently shown[21] that ^{15}N $R_{1\rho}$ rate constants in microcrystalline ubiquitin depend strongly on the precipitant used for crystallization (polyethylene glycol (PEG) versus MPD). This finding was attributed to *rocking motions* which were predicted from molecular-dynamics simulation of ubiquitin embedded in a crystal lattice. We can experimentally confirm small-amplitude motions across the entire protein and determine a correlation time of $\tau_s \approx$ 1-2 µs, which is very close to the correlation time of hundreds of ns predicted from the recent MD simulation.[21] Besides those low-amplitude rocking motions, we observe µs dynamics of larger amplitude (S_s^2 between 0.95 and 0.99, corresponding to an opening angle between 6° and 14° in the diffusion-in-a-cone model or a jump angle between 4° and 10° in a two-site jump model) for residues Gly10, Lys11 and Thr12 which are part of the β_1-β_2 turn (compare Figure 6). The β_1-β_2 turn was previously found to be involved in a *pincer-like* motion, as derived from RDC-based experiments in solution-state NMR, the timescale was suggested to be between 4 ns and 50 µs.[5f] Later-on that timescale was narrowed down to about (10 $\pm$ 9 µs) at room temperature, as extrapolated from relaxation dispersion measurements on super-cooled samples and dielectric relaxation experiments.[22] We propose that the dynamics of the β_1-β_2 turn, which we observe on the 1-2µs timescale for microcrystalline ubiquitin, corresponds to the suggested pincer-like motion.

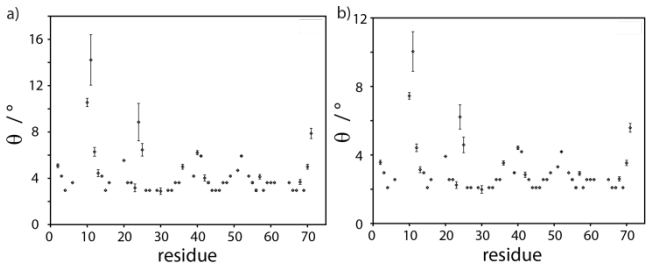

Figure 6. a) Semi-cone opening angles θ in the "motion in a cone" model that correspond to the derived order parameters S_s^2 in Fig. 2b). b) Corresponding inter-nuclear vector angle θ in a two-site jump model.

On the same 1-2 µs timescale we observed medium-amplitude motions for Glu24 and Asn25 at the N-terminus of the α-helix and Asp52 as well as for Ser20, Gln40, Gln41 and Leu71 (compare Figure 5). In solution-state NMR ^{15}N $R_{1\rho}$ relaxation dispersion measurements, Asn25 was found to be involved in a chemical exchange process with a rate constant of k_{ex} = 25000 s^{-1} at 280 K, corresponding to the 40 µs timescale.[23] A very similar timescale was found recently in multiple-quantum based experiments.[24] At 300 K this would correspond roughly to k_{ex} = 100000 s^{-1} and a 10 µs timescale, following Arrhenius law and assuming that

every 10 K the rate constant doubles as a rough approximation. This timescale is similar to the 1-2 µs timescale observed in our study. The Glu24 resonance is very weak in solution-state NMR $^{1}H^{15}N$- HSQC spectra, rationalized by even stronger exchange effects, R_{ex}, due to conformational dynamics and concomitant severe line broadening. Conformational dynamics for Ile23 and Asn25 was observed also by solid-state NMR $R_{1\rho}$ relaxation dispersion measurements, but on a slower timescale, with a fitted exchange constant of k_{ex} = 8600±1700 s^{-1}.[25]

The conformational dynamics observed for Asn25 are related to the conformational-exchange process reported for Asp52/ Gly53 and Glu24,[23-25] which is manifested as conformational variability in complexes with de-ubiquinating enzymes as well as for the ubiquitin structure crystallized in MPD (pdb code: 3ONS).[26] Here the Asp52/ Gly53 peptide plane is flipped and the side-chain conformation for Glu24 is altered compared to the ubiquitin X-ray structure (1UBQ),[27] crystallized in PEG or the solution NMR structure (1d3z),[28] but the structure is very similar otherwise. Recently, using a combination of solution-state NMR relaxation-dispersion measurements and computational methods, the Asp52 / Gly53 peptide plane flip was linked to a collective global motion of the ground state of ubiquitin,[29] involving a subtle contraction and expansion of ubiquitin, depending on the orientation of the peptide plane, albeit occurring on a slower timescale of 55 µs at 4°C, which would correspond to a timescale of about 10 µs at 23°C. It is interesting that the rocking motion in microcrystalline ubiquitin is observed at a very similar timescale and may therefore be related to the suggested subtle contraction and expansion of ubiquitin which may also appear in the crystal lattice.

The amplitudes of motion which we observe for micro-crystalline ubiquitin appear reduced compared to RDC-derived results from solution-state NMR measurements,[5e] which are sensitive to motions on all timescales that alter anisotropic interactions.[7] However, considering the microcrystalline character of the sample, our finding of reduced amplitudes of motion compared to solution may not be surprising and in a naïve picture motion observed in a microcrystalline sample could be considered as a lower boundary of dynamics that must be present also in solution. The details of the dynamics, however, depends on the context of the microcrystalline solid and higher ^{15}N $R_{1\rho}$ rate constants were observed for microcrystalline ubiquitin with PEG as crystallization agent rather than MPD (as used in our study).[21]

Temperature dependence of ^{15}N $R_{1\rho}$ ratio supports the finding of low µs dynamics.

To prove the existence of uniform small to medium-amplitude dynamics on the low µs timescale in microcrystalline ubiquitin, we varied the experimental temperature and compared the ratio of ^{15}N $R_{1\rho}$ constants (60 kHz/90 kHz) at different temperatures. To sample a wider temperature range we had to restrict the measurements to a maximum MAS frequency of 90 kHz, as at 110 kHz lowering the temperature was not possible for technical reasons. Lowering the temperature should slow down the dynamic process, and according to the simulated ratio of ^{15}N $R_{1\rho}$ rate constants (Figure 7b) we expect an increase in the ^{15}N $R_{1\rho}$ ratio, consistent with a slower timescale. That is what we observe experimentally (Figure 7c). On the other hand, when increasing the temperature, the dynamic process should become faster and the ^{15}N $R_{1\rho}$ ratio should be shifted closer to 1, consistent with a faster timescale. That is what we find experimentally (Figure 7d). In fact, as we observe a shift for the ^{15}N $R_{1\rho}$ ratios upon a small change in temperature, this underlines that the observed dynamic process must have indeed a timescale lying between a timescale of around 10 µs resulting in a ^{15}N $R_{1\rho}$ ratio of 2 to 2.5 and a timescale of around 100 ns resulting in a ^{15}N $R_{1\rho}$ ratio close to 1 (compare Figure 1c and 7b).

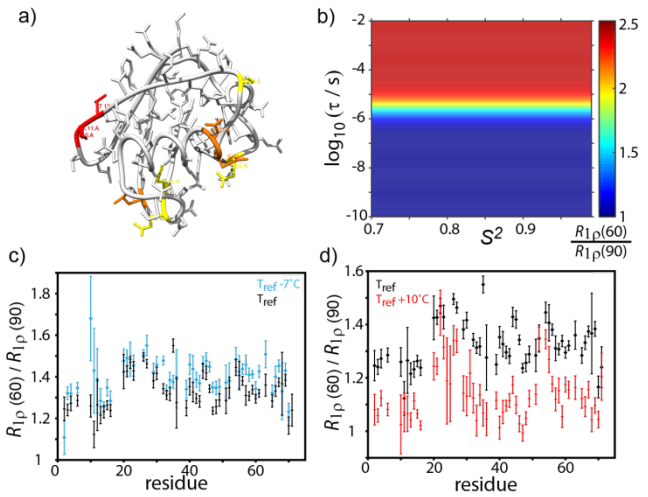

Figure 7. a) Structure of ubiquitin crystallized in MPD (pdb code: 3ONS). Residues showing larger amplitude motions in our results are color-coded in red (Gly10, Lys11 and Thr12, (motion in a cone model) semi-cone opening angle θ between 6° and 14°), orange (*θ* between 6°-10°, Glu24, Asn25 and Leu71) and yellow (*θ* between 5°-8°, Ser 20, Gln 40, Gln 41 and Asp 52). b) Simulated ratio of ^{15}N $R_{1\rho}$ at 850 MHz and 60 kHz MAS versus 90 kHz MAS, $R_{1\rho}$(60 kHz)/$R_{1\rho}$(90 kHz). c) The experimental ratio of $R_{1\rho}$(60 kHz)/$R_{1\rho}$(90 kHz) measured at 23±1°C (reference, black) is compared to the measured ratio at a 7°C lower temperature (blue) and (d) to the ratio at 10°C higher temperature (red)..

Conclusions

To summarize, we have measured ^{15}N $R_{1\rho}$ rate constants in a MAS frequency-dependent manner, with MAS frequencies between 60 and 110 kHz. We observe a MAS-dependent decrease of ^{15}N $R_{1\rho}$ rate constants. A temperature effect and coherent contributions were excluded. A simplified and robust approach to detect hundreds of ns to low µs dynamics and slow timescale (ns-µs) correlation times from the ratios of MAS dependent ^{15}N $R_{1\rho}$ rate constants was employed, applicable when ns motion is of small amplitude only as inferred from the ^{15}N R_1 data. The observed MAS dependence points to internal dynamics on a 1-2 µs timescale with low amplitude for most residues ($S_s^2 \geq 0.995$), corresponding to a semi-cone opening angle $\theta \leq 4°$ for a diffusion in a cone model. On the same 1-2 µs timescale, we find larger amplitude motions for the β_1-β_2 turn (Gly10, Lys11 and Thr12), the N-terminus of the α-helix and the region around Asp52, previously found to be involved in a hydrogen-bond reordering process. The presented approach can provide simplified access to protein dynamics in the low µs time window, difficult to study by solution-state NMR methods. It can be applied to a variety of protein samples, including e.g. microcrystalline samples or sedimented samples of larger complexes or membrane proteins.

Experimental Section

1. Sample preparation

Two different samples of [^{2}H, ^{13}C ,^{15}N] -labeled ubiquitin, one with fully back-exchanged amide protons (dubbed NH(100%) in the following) and the second one with only about 20% of amides back-exchanged, dubbed NH(20%), were prepared. Ubiquitin was expressed and crystallized in the presence of 2-methyl-2,4-pentanediol (MPD, purchased from Sigma Aldrich, USA) as described previously.[30] For the NH (100%) sample protonated MPD was used, for the NH(20%) sample deuterated MPD was used which was produced in house.

2. NMR spectroscopy

^{15}N relaxation experiments (^{15}N R_1 and ^{15}N $R_{1\rho}$) on uniformly [^{2}H, ^{13}C, ^{15}N] -labeled ubiquitin with 100% of NH back-exchanged were recorded at magnetic field strength of 20 T, corresponding to a ^{1}H Larmor frequency of 850 MHz, and at MAS frequencies of 60, 90 and 110 kHz, using a Bruker 0.7 mm solid-state NMR probe. Spectra were referenced to MPD with a chemical shift at 4.1 ppm. The sample temperature was determined to be 23±1°C, according to the up-field water line,[14] except where otherwise indicated.

^{15}N R_1 rate constants were measured using the pulse scheme shown in Figure S1a. The magnetization decay was sampled for four different relaxation delays, at 0 s (reference), 10 s, 20 s, 25 s and 30 s and compared to the reference experiments.

^{15}N $R_{1\rho}$ rate constants were measured using the pulse scheme shown in Figure S1b and a spin-lock RF amplitude of 13 kHz. The maximum spin-lock period was 320 ms (at 60 kHz MAS) and 400 ms (at 90 and 110 kHz MAS).

3. Analysis of spectra and relaxation decay curves

Data were analyzed using the CCPN Analysis software (version 2.4.2).[31] Decay rate constants were analyzed using the "Follow intensity changes" feature in CCPN, errors were analyzed using the covariance method within CCPN.

4. Model-free analysis

A model-free analysis of internal protein dynamics in the solid state was performed using dedicated MATLAB scripts and the ^{15}N $R_{1\rho}$ and ^{15}N R_1 equations applicable to the solid state, see Eq. (1) and Kurbanov et al. for the derivation.[15b] Spectral densities as derived by the model-free approach[12] and adapted to the solid state,[15b] with $J(\omega) = \frac{2}{5} S_f^2 (1 - S_s^2) \frac{\tau_s}{1+(\omega\tau_s)^2}$, were used to express the relaxation-rate constants with two free parameters per residue, the order parameter, S_s^2, and the internal correlation time τ_s. The fast timescale order parameter was determined from $S_f^2 = S_{\mathrm{REDOR}}^2 / S_s^2$, with the experimental S_{REDOR}^2 taken from ref. [18]. As explained in detail in the Results section, under this approximation the ratio of ^{15}N $R_{1\rho}$ rate constants becomes independent from S_s^2 and S_f^2. Therefore, the ratio of ^{15}N $R_{1\rho}$ rate constants, measured at different MAS frequencies depends only on a single parameter, namely the internal correlation time τ_s. For each residue, the correlation time τ_s was fitted to the ratio of ^{15}N $R_{1\rho}$ rate constants measured at 60 kHz and 110 kHz, and ^{15}N $R_{1\rho}$ rate constants at 90 kHz versus 110 kHz and 60 kHz versus 90 kHz. (By that we achieve that each data set is used two times and has therefore equal weight in the fit). Ratios of ^{15}N $R_{1\rho}$ rate constants were fitted using a grid-based approach: ^{15}N $R_{1\rho}$ ratios were calculated for an array of correlation times, τ_s, first in a wider grid with correlation times between 10^{-10} s and 10^{-2} s, in steps of 0.001 increments in the exponent to get an estimate of τ_s. Second, ratios of ^{15}N $R_{1\rho}$ rate constants were fitted to a narrower grid, calculated for correlation times τ_s between 10^{-8} and 10^{-4} s, which were incremented in steps of 0.0001 in the exponent. The best-fit point on the grid was determined using a normalized least-square χ^2 minimization. Errors of the fitted correlation time τ_s were derived by drawing randomly ^{15}N $R_{1\rho}$ from a Gaussian distribution centered around the measured experimental value and with a standard deviation equal to the experimental error (compare Table S1). These random seeds were used as input values for the fit of τ_s values, as described above. This was repeated n = 1000 times, generating a distribution of τ_s values, the standard deviation of this distribution was taken as the error on τ_s .

To determine the slow timescale order parameter, S_s^2, for each residue, we fitted S_s^2 to the set of experimental ^{15}N $R_{1\rho}$ rate constants, measured at 60, 90 and 110 kHz MAS frequency using a grid-based approach, very similar to the one described above. A two-

dimensional grid was created for values of S_s^2, ranging between 0.7 and 1.0 with an increment of 0.001, and τ_s between 10^{-8} and 10^{-4} s, which were incremented in steps of 0.0001 in the exponent. For the χ^2 minimization, the correlation time τ_s was kept fixed at the value determined from the fit to the ratio of ^{15}N $R_{1\rho}$ rate constants, described above. Thus, the only free parameter in the fit was S_s^2. To determine the error on S_s^2, n = 1000 random seeds from a Gaussian distribution centered at the experimental ^{15}N $R_{1\rho}$ rate and with a standard deviation equal to the experimental error were taken as input to the fit of S_s^2. This was repeated m = 100 times for different input values of τ_s, drawn from the distribution of τ_s values, described above.

The model-free order parameter, S_s^2, was translated to the restricted rotational diffusion (*diffusion-in-a-cone*) model with a semi-cone opening angle, θ, which relates to the order parameter S by $S = \frac{1}{2}\cos\theta\,(1 + \cos\theta)$,[12a] as well as to a *two-site jump* model with a jump angle, θ, between the two different orientations of the NH vector; equal populations were assumed for both vector orientations. The order parameter S_s^2 is here related to θ by $S^2 = \frac{1}{2}(3\cos^2\theta - 1)$.[12a]

To evaluate the quality of the fit, ^{15}N $R_{1\rho}$ rate constants were back-calculated using the fitted $(S_s^2,\ \tau_s)$ values and compared to the experimental input values.

Acknowledgements

We would like to thank Guido Grassi for producing the deuterated MPD and Emilie Testori for help with the crystallization of ubiquitin samples. We also thank Andreas Hunkeler and Alexander Däpp for technical support and Francesco Ravotti and Albert A. Smith for helpful discussions. This research was funded by the EU Marie-Curie program (grant number 627767, to N.L.), the Swiss National Science Foundation (grant number SNF 200020-159707, to B.M.) and ETH Zurich (grant number ETH-45 13-2, to B.M.).

Keywords: Biophysics • NMR spectroscopy • protein dynamics • ubiquitin • microsecond timescale

[1] a) A. Mittermaier, L. E. Kay, *Science* **2006**, *312*, 224-228; b) D. D. Boehr, D. McElheny, H. J. Dyson, P. E. Wright, *Science* **2006**, *313*, 1638-1642; c) A. G. Palmer, 3rd, *Acc. Chem. Res.* **2015**, *48*, 457-465; dR. Rosenzweig, L. E. Kay, *J. Am. Chem. Soc.* **2015**.

[2] a) L. E. Kay, D. A. Torchia, A. Bax, *Biochemistry* **1989**, *28*, 8972-8979; b) J. W. Peng, G. Wagner, *Methods Enzymol.* **1994**, *239*, 563-596; c) F. A. Mulder, N. R. Skrynnikov, B. Hon, F. W. Dahlquist, L. E. Kay, *J. Am. Chem. Soc.* **2001**, *123*, 967-975; d) A. G. Palmer, 3rd, F. Massi, *Chem. Rev.* **2006**, *106*, 1700-1719.

[3] D. Ban, A. D. Gossert, K. Giller, S. Becker, C. Griesinger, D. Lee, *J. Magn. Res.* **2012**, *221*, 1-4.

[4] N. A. Lakomek, C. Fares, S. Becker, T. Carlomagno, J. Meiler, C. Griesinger, *Angew. Chem. Int. Ed. Engl.* **2005**, *44*, 7776-7778.

[5] a) J. R. Tolman, J. M. Flanagan, M. A. Kennedy, J. H. Prestegard, *Nat. Struct. Biol.* **1997**, *4*, 292-297; b) W. Peti, J. Meiler, R. Bruschweiler, C. Griesinger, *J. Am. Chem. Soc.* **2002**, *124*, 5822-5833; c) G. M. Clore, C. D. Schwieters, *J. Am. Chem. Soc.* **2004**, *126*, 2923-2938; d) G. M. Clore, C. D. Schwieters, *J. Mol. Biol.* **2006**, *355*, 879-886; e) N. A. Lakomek, K. F. A. Walter, C. Fares, O. F. Lange, B. L. de Groot, H. Grubmuller, R. Bruschweiler, A. Munk, S. Becker, J. Meiler, C. Griesinger, *J. Biomol. NMR* **2008**, *41*, 139-155; f) O. F. Lange, N. A. Lakomek, C. Fares, G. F. Schroder, K. F. Walter, S. Becker, J. Meiler, H. Grubmuller, C. Griesinger, B. L. de Groot, *Science* **2008**, *320*, 1471-1475; g) L. Yao, B. Vogeli, D. A. Torchia, A. Bax, *J. Phys. Chem. B* **2008**, *112*, 6045-6056; h) L. Salmon, G. Bouvignies, P. Markwick, N. Lakomek, S. Showalter, D. W. Li, K. Walter, C. Griesinger, R. Bruschweiler, M. Blackledge, *Angew. Chem. Int. Ed. Engl.* **2009**, *48*, 4154-4157; i) A. S. Maltsev, A. Grishaev, J. Roche, M. Zasloff, A. Bax, *J. Am. Chem. Soc.* **2014**, *136*, 3752-3755; j) A. Carlon, E. Ravera, W. Andralojc, G. Parigi, G. N. Murshudov, C. Luchinat, *Prog. Nucl. Magn. Reson. Spectrosc.* **2016**, *92-93*, 54-70.

[6] J. L. Lorieau, A. E. McDermott, *J. Am. Chem. Soc.* **2006**, *128*, 11505-11512.

[7] P. Schanda, M. Ernst, *Prog. Nucl. Magn. Reson. Spectrosc.* **2016**, *96*, 1-46.

[8] a) V. Chevelkov, U. Fink, B. Reif, *J. Am. Chem. Soc.* **2009**, *131*, 14018-14022; b) P. Schanda, B. H. Meier, M. Ernst, *J. Am. Chem. Soc.* **2010**, *132*, 15957-15967; c) J. R. Lewandowski, J. Sein, M. Blackledge, L. Emsley, *J. Am. Chem. Soc.* **2010**, *132*, 1246-1248.

[9] a) B. Reif, C. P. Jaroniec, C. M. Rienstra, M. Hohwy, R. G. Griffin, *J. Magn. Reson.* **2001**, *151*, 320-327; b) V. Chevelkov, B. J. van Rossum, F. Castellani, K. Rehbein, A. Diehl, M. Hohwy, S. Steuernagel, F. Engelke, H. Oschkinat, B. Reif, *J. Am. Chem. Soc.* **2003**, *125*, 7788-7789.

[10] a) D. H. Zhou, G. Shah, M. Cormos, C. Mullen, D. Sandoz, C. M. Rienstra, *J. Am. Chem. Soc.* **2007**, *129*, 11791-11801; b) D. H. Zhou, J. J. Shea, A. J. Nieuwkoop, W. T. Franks, B. J. Wylie, C. Mullen, D. Sandoz, C. M. Rienstra, *Angew. Chem. Int. Ed. Engl.* **2007**, *46*, 8380-8383; c) I. Bertini, L. Emsley, M. Lelli, C. Luchinat, J. Mao, G. Pintacuda, *J. Am. Chem. Soc.* **2010**, *132*, 5558-5559; d) M. J. Knight, A. J. Pell, I. Bertini, I. C. Felli, L. Gonnelli, R. Pierattelli, T. Herrmann, L. Emsley, G. Pintacuda, *Proc. Natl. Acad. Sci. U. S. A.* **2012**, *109*, 11095-11100; e) V. Agarwal, S. Penzel, K. Szekely, R. Cadalbert, E. Testori, A. Oss, J. Past, A. Samoson, M. Ernst, A. Bockmann, B. H. Meier, *Angew. Chem. Int. Ed. Engl.* **2014**, *53*, 12253-12256.

[11] a) A. Krushelnitsky, T. Zinkevich, D. Reichert, V. Chevelkov, B. Reif, *J. Am. Chem. Soc.* **2010**, *132*, 11850-11853; b) J. R. Lewandowski, H. J. Sass, S. Grzesiek, M. Blackledge, L. Emsley, *J. Am. Chem. Soc.* **2011**, *133*, 16762-16765.

[12] a) G. Lipari, A. Szabo, *J. Am. Chem. Soc.* **1982**, *104*, 4546-4559; b) G. M. Clore, A. Szabo, A. Bax, L. E. Kay, P. C. Driscoll, A. M. Gronenborn, *J. Am. Chem. Soc.* **1990**, *112*, 4989-4991.

[13] N. Tjandra, S. E. Feller, R. W. Pastor, A. Bax, *J. Am. Chem. Soc.* **1995**, *117*, 12562-12566.

[14] A. Bockmann, C. Gardiennet, R. Verel, A. Hunkeler, A. Loquet, G. Pintacuda, L. Emsley, B. H. Meier, A. Lesage, *J. Biomol. NMR* **2009**, *45*, 319-327.

[15] a) U. Haeberlen, J. S. Waugh, *Phys. Rev.* **1969**, *185*, 420-429; b) R. Kurbanov, T. Zinkevich, A. Krushelnitsky, *J. Chem. Phys.* **2011**, *135*, 184104.

[16] S. F. Lienin, T. Bremi, B. Brutscher, R. Bruschweiler, R. R. Ernst, *J. Am. Chem. Soc.* **1998**, *120*, 9870-9879.

[17] a) A. Krushelnitsky, T. Zinkevich, B. Reif, K. Saalwachter, *J. Magn. Reson.* **2014**, *248*, 8-12; b) T. Zinkevich, V. Chevelkov, B. Reif, K. Saalwachter, A. Krushelnitsky, *J. Biomol. NMR* **2013**, *57*, 219-235.

[18] J. D. Haller, P. Schanda, *J. Biomol. NMR* **2013**, *57*, 263-280.

[19] J. M. Lamley, M. J. Lougher, H. J. Sass, M. Rogowski, S. Grzesiek, J. R. Lewandowski, *Phys. Chem. Chem. Phys.* **2015**, *17*, 21997-22008.

[20] A. A. Smith, E. Testori, R. Cadalbert, B. H. Meier, M. Ernst, *J. Biomol. NMR* **2016**, *65*, 171-191.
[21] P. Ma, Y. Xue, N. Coquelle, J. D. Haller, T. Yuwen, I. Ayala, O. Mikhailovskii, D. Willbold, J. P. Colletier, N. R. Skrynnikov, P. Schanda, *Nat. Commun.* **2015**, *6*, 8361.
[22] D. Ban, M. Funk, R. Gulich, D. Egger, T. M. Sabo, K. F. A. Walter, R. B. Fenwick, K. Giller, F. Pichierri, B. L. de Groot, O. F. Lange, H. Grubmuller, X. Salvatella, M. Wolf, A. Loidl, R. Kree, S. Becker, N. A. Lakomek, D. Lee, P. Lunkenheimer, C. Griesinger, *Angew. Chem. Int. Ed. Engl.* **2011**, *50*, 11437-11440.
[23] F. Massi, M. J. Grey, A. G. Palmer, *Protein Sci.* **2005**, *14*, 735-742.
[24] N. Salvi, S. Ulzega, F. Ferrage, G. Bodenhausen, *J. Am. Chem. Soc.* **2012**, *134*, 2481-2484.
[25] P. Ma, J. D. Haller, J. Zajakala, P. Macek, A. C. Sivertsen, D. Willbold, J. Boisbouvier, P. Schanda, *Angew. Chem. Int. Ed. Engl.* **2014**, *53*, 4312-4317.
[26] K. Y. Huang, G. A. Amodeo, L. A. Tong, A. McDermott, *Protein Sci.* **2011**, *20*, 630-639.
[27] S. Vijaykumar, C. E. Bugg, W. J. Cook, *J. Mol. Biol.* **1987**, *194*, 531-544.
[28] G. Cornilescu, J. L. Marquardt, M. Ottiger, A. Bax, *J. Am. Chem. Soc.* **1998**, *120*, 6836-6837.
[29] C. A. Smith, D. Ban, S. Pratihar, K. Giller, M. Paulat, S. Becker, C. Griesinger, D. Lee, B. L. de Groot, *Proc. Natl. Acad. Sci. U. S. A.* **2016**, *113*, 3269-3274.
[30] M. Schubert, T. Manolikas, M. Rogowski, B. H. Meier, *J. Biomol. NMR* **2006**, *35*, 167-173.
[31] W. F. Vranken, W. Boucher, T. J. Stevens, R. H. Fogh, A. Pajon, P. Llinas, E. L. Ulrich, J. L. Markley, J. Ionides, E. D. Laue, *Proteins: Struct. Funct. Bioinf.* **2005**, *59*, 687-696.